

Cross-dimensional valley excitons from Förster coupling in arbitrarily twisted stacks of monolayer semiconductors

Ci Li^{1,2} and Wang Yao^{1,2,*}

¹*Department of Physics, The University of Hong Kong, Hong Kong, China*

²*HKU-UCAS Joint Institute of Theoretical and Computational Physics at Hong Kong, China*

In stacks of transition metal dichalcogenide monolayers with arbitrary twisting angles, we explore a new class of bright excitons arising from the pronounced Förster coupling, whose dimensionality is tuned by its in-plane momentum. The low energy sector at small momenta is two-dimensional, featuring a Mexican Hat dispersion, while the high energy sector at larger momenta becomes three-dimensional (3D) with sizable group velocity both in-plane and out-of-plane. By choices of the spacer thickness, interface exciton mode strongly localized at designated layers can emerge out of the cross-dimensional bulk dispersion for a topological origin. Step-edges in spacers can be exploited for engineering lateral interfaces to enable interlayer communication of the topological interface exciton. Combined with the polarization selection rule inherited from the monolayer building block, these exotic exciton properties open up new opportunities for multilayer design towards 3D integration of valley exciton optoelectronics.

Atomically thin transition metal dichalcogenides (TMDs) have provided an exciting platform for studying excitons in the two-dimensional (2D) limit. Band-edge electrons and holes from the degenerate $\pm K$ valleys at the Brillouin zone corners form tightly bound Wannier excitons with optical selection rules for manipulating the valley pseudospin [1–10]. The small Bohr radius $\sim O(1)$ nm [11–13] further underlies a pronounced electron-hole (e-h) Coulomb exchange at finite center-of-mass (COM) momentum that can transfer bright excitons between these two valleys, with a coupling phase dependent on momentum direction [7, 14–16]. This realizes a sizable coupling between exciton’s valley pseudospin and COM degrees of freedom, splitting the exciton dispersion into two branches having linearly polarized optical dipole longitudinal (L) and transverse (T) to exciton momentum respectively [7, 15, 17–20]. Notably, the L branch is a massless one with group velocity proportional to Coulomb strength, whose sensitive dependence on surrounding dielectric [21, 22] can lead to exotic properties of ground state excitons in a monolayer TMD on patterned substrates [23, 24].

Reassembly of monolayer building blocks by van der Waals stacking further provides versatile opportunities to explore exciton physics and optoelectronic functionalities. By its long-range nature, the e-h Coulomb exchange can also non-locally transfer exciton or e-h pair, which is well known as the Förster coupling or Förster energy transfer [25]. Efficient Förster energy transfer between excitons in a TMD monolayer and adjacent nanostructures have been found [26], promising sensing and imaging applications [27, 28]. The Förster coupling in principle allows exciton to propagate out-of-plane in a stack of layers of homogeneous excitonic resonance, even when charge hopping is completely quenched by spacer layers or crystalline misalignment. This implies an intriguing yet unexplored possibility to engineer the dimensionality of excitons separately from that of charge carriers.

Here we discover a new class of bright excitons of cross-dimensionality, introduced by the strong Förster coupling in van der Waals stacks of TMDs monolayers of quenched charge hopping. Exciton’s in-plane COM momentum k_{\parallel} serves as the parameter to tune its dimensionality, which crosses from 2D at small k_{\parallel} to 3D at large k_{\parallel} . The low-energy sector features a series of 2D subbands well separated in energy, where the energy minimum has a ring geometry. In the high-energy sector, excitons acquire significant group velocity both in-plane and out-of-plane. As the Förster coupling concerns the momentum of exciton only, rather than that of the electron or hole, the dispersion and polarization selection rules of the cross-dimensional exciton are immune to the arbitrary rotation of any layer in the stack. We further show that, by choices of the spacer thickness, interface exciton mode strongly localized at designated layers can emerge out of the cross-dimensional bulk dispersion, with a topological origin that can be mapped to the Su-Schrieffer-Heeger (SSH) chain [29, 30]. Step-edges in spacers can be exploited for efficient interlayer transfer of the topological interface exciton upon its lateral transport. These findings point to a new avenue towards valley excitonic circuits of multilayer design for high-level 3D integration.

Excitonic Förster coupling in arbitrarily twisted multilayer - We consider stack of monolayers of the same TMD compound, all separated by thin hBN spacers such that charge hopping is completely quenched (Fig. 1). The Hamiltonian of valley excitons can be written as

$$H = \frac{\hbar^2 k_{\parallel}^2}{2m_X} + \sum_l H_{\text{intra}}^l + \sum_{l,l'} H_{\text{inter}}^{l,l'}. \quad (1)$$

$\mathbf{k}_{\parallel} = (k_{\parallel} \cos \varphi, k_{\parallel} \sin \varphi)$ is the COM momentum in-plane. H_{intra} and H_{inter} denote respectively the intra- and inter-layer electron-hole (e-h) Coulomb exchange.

H_{intra} consists of terms annihilating an e-h pair in one valley while creating one in the same or opposite valley,

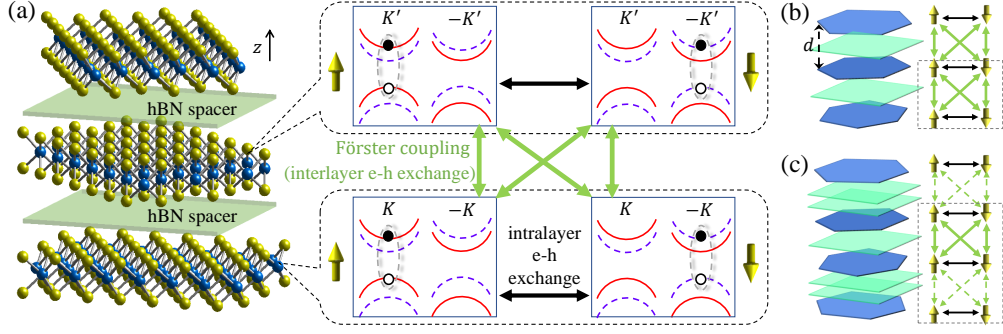


FIG. 1. (Color online)(a) Schematic of an arbitrarily twisted stack of monolayer TMDs, where hBN spacers quench charge hopping. The two valley configurations of bright excitons in each layer are coupled by the intralayer electron-hole (e-h) Coulomb exchange (black arrows). Green arrows denote the Förster coupling, i.e., the interlayer e-h exchange, which couples bright exciton states from different layers. Yellow arrows represent the valley pseudospin. (b)-(c) Schematics of exemplary stacking configurations, and the corresponding Förster coupling between exciton valley configurations from different TMD layers. As the Förster coupling conserves the exciton momentum in-plane, at each COM k_{\parallel} the exciton states form a quasi-one-dimensional (1D) chain. Only the nearest neighbor Förster coupling is displayed here, where the dashed arrow denotes weaker coupling strength due to the thicker spacer.

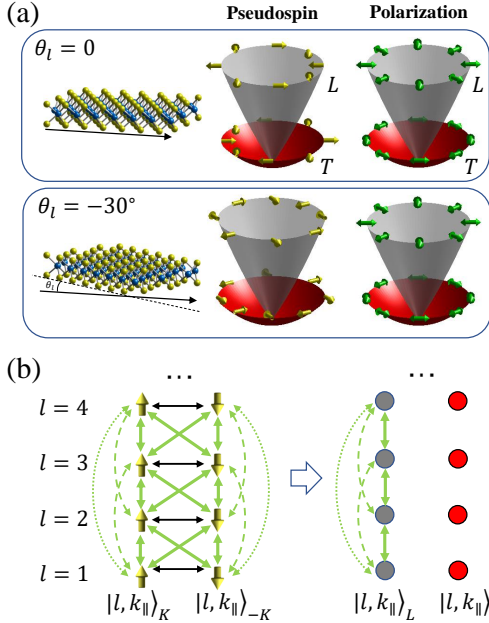


FIG. 2. (Color online)(a) L and T exciton branches split by the electron-hole exchange in a monolayer TMD. The left column displays the valley pseudospin texture (single-head arrow). In the gauge chosen (c.f. text), the pseudospin texture rotates with the crystalline axis of the corresponding layer. The right column displays the gauge-independent texture of the polarization of the optical dipole (double-head arrow). (b) Exciton states of a common COM momentum \mathbf{k}_{\parallel} from different layers are coupled nonlocally by the Förster coupling, forming a 1D ladder in the valley pseudospin basis. Transforming to the L and T basis, the L states are coupled by the Förster coupling into a chain, while all T states are decoupled.

with \mathbf{k}_{\parallel} conserved. In the basis $\left\{ |l, \mathbf{k}_{\parallel}\rangle_K, |l, \mathbf{k}_{\parallel}\rangle_{-K} \right\}$ denoting exciton from valley K or $-K$ of layer l , it

reads [7, 15, 17–20],

$$H_{\text{intra}}^l = \begin{pmatrix} J_{K,K} & J_{K,-K}^l \\ J_{-K,K}^l & J_{-K,-K} \end{pmatrix},$$

where

$$J_{\pm K, \pm K}^l \approx \rho(0) V(\mathbf{k}_{\parallel}) (e^{\mp i\theta_l} \mathbf{k}_{\parallel} \cdot \mathbf{d}_{cv, \pm K}) \times (e^{\mp i\theta_l} \mathbf{k}_{\parallel} \cdot \mathbf{d}_{cv, \pm K})^*. \quad (2)$$

$\rho(0) \sim a_B^{-2}$ is the probability for electron and hole to overlap in an exciton of Bohr radius a_B . $\mathbf{d}_{cv, \pm K} = d_0(\pm \hat{\mathbf{x}} - i\hat{\mathbf{y}})$ is the optical transition dipole between conduction and valence band edges, which is $\sigma+$ and $\sigma-$ polarized at K and $-K$ respectively. θ_l is the twist angle of layer l in the real space. Taking an unscreened form for the Coulomb potential $V(\mathbf{k}_{\parallel})$ then leads to $J_{K,K}^l(-K,-K) = J_{K,K}(-K,-K) = J_{K,K}^l$, where $K = 4\pi/3a$, a being TMD's lattice constant, and $J \sim 1$ eV can be extracted from first principle wavefunctions and exciton spectrum [11, 15, 17, 18]. The off-diagonal term has the same magnitude, but with a phase depending on the direction of \mathbf{k}_{\parallel} ,

$$J_{K,-K}^l = (J_{-K,K}^l)^* = -J_{K,K}^l e^{-2i(\theta_l + \varphi)}.$$

θ_l appears as a global phase under the gauge choice that the valley pseudospin texture in the eigen branches of H_{intra}^l rotates together with the lattice (c.f. Fig. 2(a), and Supplementary [33]):

$$\begin{aligned} |l, \mathbf{k}_{\parallel}\rangle_L &= \frac{-e^{-i(\theta_l + 2\varphi)} |l, \mathbf{k}_{\parallel}\rangle_K + e^{i\theta_l} |l, \mathbf{k}_{\parallel}\rangle_{-K}}{\sqrt{2}}, \\ |l, \mathbf{k}_{\parallel}\rangle_T &= \frac{e^{-i\theta_l} |l, \mathbf{k}_{\parallel}\rangle_K + e^{i(2\varphi + \theta_l)} |l, \mathbf{k}_{\parallel}\rangle_{-K}}{\sqrt{2}}. \end{aligned} \quad (3)$$

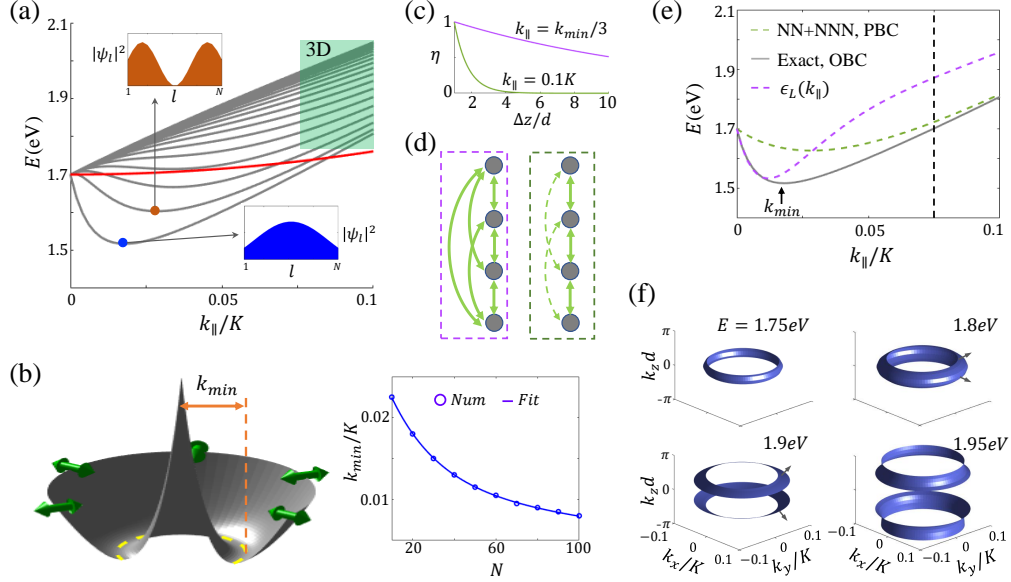


FIG. 3. (Color online) (a) Exciton dispersion for a stack of $N = 20$ TMDs layers with a uniform interlayer distance $d = 1$ nm (corresponding to single layer hBN spacer). Grey (red) denotes the L (T) branch excitons (c.f. Fig. 2(a)). Förster coupling of L excitons leads to a series of subbands well separated in the low energy sector. Insets show layer distribution of exciton wavefunction in the two lowest subbands. (b) Left: Mexican Hat dispersion of the lowest subband, k_{\min} denoting the radius of the energy minima ring. Right: k_{\min} as a function of the layer number N . (c) Förster coupling range indicated by the plot of $\eta \equiv \exp[k_{\parallel}(\Delta z - d)]$ as a function of out-of-plane distance Δz , at two representative k_{\parallel} . (d) Chain of Förster coupled exciton states from different layers at a common k_{\parallel} . The coupling is highly nonlocal at small k_{\parallel} (left), compared to that at large k_{\parallel} (right). (e) The lowest exciton subband (solid curve), in comparison with two approximations (dashed curves) for small and large k_{\parallel} regions respectively (Eqs. (6) and (7)). (f) Energy isosurfaces of the 3D exciton dispersion in the high energy sector (green shaded in (a)), plotted using Eq. (7) that keeps nearest-neighbor (NN) and next nearest-neighbor (NNN) Förster coupling. Arrows denote the direction of exciton group velocity.

The optical dipoles of these eigenstates, nonetheless, are gauge invariant quantities that remain longitudinal and transverse to \mathbf{k}_{\parallel} in the two branches respectively [15, 32], regardless of the twisting angle. This is guaranteed by the rotational symmetry of the monolayer.

Likewise, the interlayer e-h exchange, i.e., Förster coupling, consists of \mathbf{k}_{\parallel} conserving terms that annihilate an e-h pair in layer l while creating one in a different layer l' . It can be expressed in the same basis as,

$$H_{\text{inter}}^{l,l'} = \begin{pmatrix} J_{K,K}^{l,l'} & J_{K,-K}^{l,l'} \\ J_{-K,K}^{l,l'} & J_{-K,-K}^{l,l'} \end{pmatrix}, \quad (4)$$

$$J_{K,K}^{l,l'} = \left(J_{-K,-K}^{l,l'} \right)^* \approx J \frac{k_{\parallel}}{K} e^{-k_{\parallel} \Delta z} e^{i(\theta_{l'} - \theta_l)},$$

$$J_{K,-K}^{l,l'} = \left(J_{-K,K}^{l,l'} \right)^* \approx -J \frac{k_{\parallel}}{K} e^{-k_{\parallel} \Delta z} e^{-i(\theta_l + \theta_{l'}) - 2i\varphi}.$$

The dependence on $\Delta z \equiv |\mathbf{z}_l - \mathbf{z}_{l'}|$, i.e., vertical distance between layer l and l' , comes from the 3D form of Coulomb interaction [31] (see Supplementary [33]). From the $k_{\parallel} e^{-k_{\parallel} \Delta z}$ dependence, we note that Förster coupling can be neglected inside the light cone where k_{\parallel} is close to zero. At modestly small k_{\parallel} , a finite and highly non-local coupling develops, while at large k_{\parallel} it becomes short-ranged with large magnitude.

The total Hamiltonian in Eq. (1) now reads,

$$H = \sum_{\lambda=L,T} \sum_l \varepsilon_{\lambda} |l, \mathbf{k}_{\parallel}\rangle_{\lambda} \langle l, \mathbf{k}_{\parallel}|_{\lambda} \quad (5)$$

$$- 2J \frac{k_{\parallel}}{K} \sum_{l,l'} e^{-k_{\parallel} \Delta z} (|l, \mathbf{k}_{\parallel}\rangle_L \langle l', \mathbf{k}_{\parallel}|_L + H.c.),$$

where $\varepsilon_L = \frac{\hbar^2 k_{\parallel}^2}{2m_X} + 2J \frac{k_{\parallel}}{K}$ and $\varepsilon_T = \frac{\hbar^2 k_{\parallel}^2}{2m_X}$. Notably, in the basis of L and T polarized excitons (Eq. (3)), H has a gauge invariant form, independent of twist angles $\{\theta_l\}$.

Cross dimensional valley exciton in the bulk - At each \mathbf{k}_{\parallel} , the L excitons from different layers are Förster coupled to form a chain (Fig. 2(b)). The Förster coupling range is inversely proportional to k_{\parallel} , so distinct behaviors at small and large momenta are expected. Fig. 3(a) plots the calculated exciton dispersions in a stack of $N = 20$ TMDs layers, separated by monolayer hBN spacer (c.f. Fig. 1(b)). T branch dispersion (red curve) remains the same as that in monolayer, as they are not affected by Förster coupling (Fig. 2(b)). In small k_{\parallel} region, Förster coupling splits the L branch into a series of subbands (grey curves) with energy separation of tens of meV. With such strong quantization freezing the out-of-plane motion, exciton remains 2D, but the dispersion is strongly renormalized. Remarkably, the lowest energy

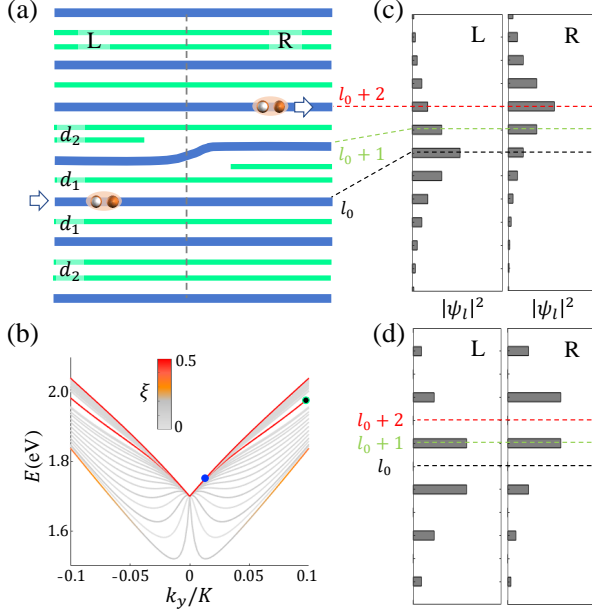


FIG. 4. (Color online)(a) Schematic of a TMD stack with an alternating thickness of spacers, mimicking the Su-Schrieffer-Heeger (SSH) chain. Layer l_0 sandwiched by two spacers of d_1 thickness is a topological interface in the SSH chain. A step-edge in the spacer layer defines a lateral boundary, where the topological interface to its right is shifted upward, becoming layer $l_0 + 2$. (b) The exciton dispersion of L branch in such a stack of $N = 31$ TMDs, with a topological interface in the middle. $d_1 = 1$ nm and $d_2 = 1.33$ nm, corresponding to one and two hBN layers, respectively. Each subband is color-coded by $\xi \equiv |\psi_l|^2 + |\psi_{l_0-1}|^2 + |\psi_{l_0+1}|^2$, where ψ_l is the normalized wavefunction on layer l . The red color highlights a topological interface mode strongly localized on layer l_0 . (c) The left (right) panel plots the layer distribution of the interface mode to the left (right) side of the step-edge, for the state marked by the blue dot on the dispersion in (b). The center of the wavefunction is displaced by two TMD layers (c.f. (a)), but still has a significant overlap to ensure efficient transmission across the step-edge, realizing an interlayer communication. (d) A similar plot for the state marked by the black dot in (b).

one features a Mexican Hat dispersion, such that the exciton ground state becomes highly degenerate (Fig. 3(b)). The energy minima ring is outside the light cone, where excitons can be scattered into the light cone by long wavelength phonon ($k_{\min} \sim 10^{-2}K$), suggesting a desirable balance between long lifetime and optical observability.

For $k_{\parallel} \leq k_{\min}$, we note that the Förster coupling is highly non-local (Fig. 3(c)), and all layers in the $N = 20$ stack are strongly coupled to each other with roughly the same order of strength. The coupling in the chain may be simplified as (Fig. 3(d)),

$$-J \frac{k_{\parallel}}{K} e^{-k_{\parallel} f d} \sum_{l, l'} (|l, \mathbf{k}_{\parallel}\rangle_L \langle l', \mathbf{k}_{\parallel}|_L + H.c.),$$

which has analytical solution of the lowest subband as

$$E_0(k_{\parallel}) = \varepsilon_L - 2J(N-1) \frac{k_{\parallel}}{K} e^{-f k_{\parallel} d}. \quad (6)$$

With a factor $f = N/3.5$ to account for the weak distance dependence of the long-range Förster coupling, Eq. (6) agrees well with the numerical solution for $k_{\parallel} \leq k_{\min}$ (c.f. Fig. 3(e)).

For $k_{\parallel} \sim 0.1K$, the subbands in Fig. 3(a) get densely packed so that motion in the out-of-plane becomes relevant. Note that at such large k_{\parallel} , the Förster coupling becomes short ranged as shown in Fig. 3(c), which can be simplified by keeping only the nearest and next-nearest neighbors (Fig. 3(d))

$$-2J \frac{k_{\parallel}}{K} \sum_{s=1}^2 e^{-s k_{\parallel} d} (|l, \mathbf{k}_{\parallel}\rangle_L \langle l+s, \mathbf{k}_{\parallel}|_L + H.c.).$$

It also has an analytical solution under periodic boundary condition (PBC),

$$E(\mathbf{k}) = \varepsilon_L - 4J \frac{k_{\parallel}}{K} (e^{-k_{\parallel} d} \cos k_z d + e^{-2k_{\parallel} d} \cos 2k_z d), \quad (7)$$

In the region $k_{\parallel} \sim 0.1K$, it agrees well with the numerical solution that keeps the full Förster coupling under open boundary condition (OBC) (Fig. 3(e)). In this high-energy sector, the dispersion becomes 3D, where exciton moves with sizable group velocity that can reach 10^5 m/s both in-plane and out-of-plane (Fig. 3(f)).

Engineering topological interface exciton by choices of spacer thickness - The near-neighbor coupled chain structure in the large k_{\parallel} limit suggests a design strategy to engineer topological features using alternating thicknesses of spacers (Fig. 1(c)). This is reminiscent of the dimerized SSH chain, where nontrivial bulk winding number leads to the emergence of topological modes at edges and interfaces [29, 30]. The latter can be engineered by breaking the periodicity of the spacer thickness pattern (see Fig. 4(a)). Fig. 4(b) shows the calculated exciton dispersions of such stack with $N = 31$ TMDs monolayers, modes strongly localized at the interface (extended in out-of-plane direction) are marked as red (grey) by color-coding.

Keeping only the nearest-neighbor Förster coupling justifiable at sufficiently large k_{\parallel} , for the stacking configuration in Fig. 4(a) (see Supplementary [33]), one can find one interface mode in the bulk spectrum gap

$$|\phi_1\rangle = \frac{1}{A} \sum_{s=1} \left(-\frac{v}{w}\right)^{s-1} [|l_{\text{dw}} - 2s + 1\rangle_L - |l_{\text{dw}} + 2s - 1\rangle_L]$$

l_{dw} represents the interface layer (domain wall) as shown in Fig. 4(a). A is the normalization factor, w and v denoting Förster coupling strength in Eq. (5) at $\Delta z = d_1$

and d_2 respectively. There are also two interface modes at the top and bottom edges of bulk spectrum,

$$|\phi_2\rangle \approx \frac{1}{2}(|l_{dw} + 1\rangle_L + |l_{dw} - 1\rangle_L) + \frac{1}{\sqrt{2}}|l_{dw}\rangle_L$$

$$|\phi_3\rangle \approx \frac{1}{2}(|l_{dw} + 1\rangle_L + |l_{dw} - 1\rangle_L) - \frac{1}{\sqrt{2}}|l_{dw}\rangle_L$$

From Fig. 4(b), we can indeed identify the three modes at large $k_{||}$. It is interesting to note that the two higher energy modes remain strongly localized over the entire $k_{||}$ region, even when the above nearest-neighbor approximation breaks down at small $k_{||}$.

The possibility to engineer such topological interface mode at designated layers further points to an interesting scenario by creating step-edges in the spacer layers while keeping the TMDs layer intact (Fig. 4(a)). The wavefunction plotted in Fig. 4(c,d) shows that the interface modes at the two sides of the step-edge have their out-of-plane distribution shifted by two TMDs layers. Their spatial overlap suggests a significant lateral transmission probability through the step-edge, upon which the exciton is also transferred across two layers. This can be exploited to realize interlayer communication of valley excitons in a multilayer design of valley excitonic circuits for 3D integration.

Acknowledgments -C.L. would like to thank D. W. Zhai, B. Fu, H. Y. Zheng, and B. B for useful discussions. This work is supported by the National Key R&D Program of China (2020YFA0309600), and Research Grant Council of Hong Kong SAR (AoE/P-701/20, HKU SRFS2122-7S05). W.Y. also acknowledges support by Tencent Foundation.

* wangyao@hku.hk

- [1] D. Xiao, G.-B. Liu, W. Feng, X. Xu, and W. Yao, Coupled spin and valley physics in monolayers of MoS₂ and other group VI dichalcogenides, *Phys. Rev. Lett.* **108**, 196802 (2012).
- [2] K. F. Mak, K. He, J. Shan, and T. F. Heinz, Control of valley polarization in monolayer MoS₂ by optical helicity, *Nat. Nanotech.* **7**, 494–498 (2012).
- [3] H. Zeng, J. Dai, W. Yao, D. Xiao, and X. Cui, Valley polarization in MoS₂ monolayers by optical pumping, *Nat. Nanotech.* **7**, 490–493 (2012).
- [4] Ting Cao, Gang Wang, Wenpeng Han, Huiqi Ye, Chuanrui Zhu, Junren Shi, Qian Niu, Pingheng Tan, Enge Wang, Baoli Liu, and Ji Feng, Valley-selective circular dichroism of monolayer molybdenum disulphide, *Nat. Commun.* **3**, 887 (2012).
- [5] Aaron M. Jones, Hongyi Yu, Nirmal J. Ghimire, Sanfeng Wu, Grant Aivazian, Jason S. Ross, Bo Zhao, Jiaqiang Yan, David G. Mandrus, Di Xiao, Wang Yao, and Xiaodong Xu, Optical generation of excitonic valley coherence in monolayer WSe₂, *Nat. Nanotech.* **8**, 634–638 (2013).
- [6] J. Kim, X. P. Hong, C. H. Jin, Su-Fei Shi, Chih-Yuan S. Chang, Ming-Hui Chiu, Lain-Jong Li, and F. Wang, Ultrafast generation of pseudo-magnetic field for valley excitons in WSe₂ monolayers, *Science* **346**, 1205–1208 (2014).
- [7] H. Yu, X. Cui, X. Xu, and W. Yao, Valley excitons in two-dimensional semiconductors, *Natl. Sci. Rev.* **2**, 57–70 (2015).
- [8] G. Wang, X. Marie, B. L. Liu, T. Amand, C. Robert, F. Cadiz, P. Renucci, and B. Urbaszek, Control of exciton valley coherence in transition metal dichalcogenide monolayers, *Phys. Rev. Lett.* **117**, 187401 (2016).
- [9] Z. Ye, D. Sun, and T. F. Heinz, Optical manipulation of valley pseudospin, *Nat. Phys.* **13**, 26–29 (2016).
- [10] Kai Hao, Galan Moody, Fengcheng Wu, Chandriker Kavir Dass, Lixiang Xu, Chang-Hsiao Chen, Liuyang Sun, Ming-Yang Li, Lain-Jong Li, Allan H. MacDonald, and Xiaoqin Li, Direct measurement of exciton valley coherence in monolayer WSe₂, *Nat. Phys.* **12**, 677–682 (2016).
- [11] D. Y. Qiu, F. H. da Jornada, and S. G. Louie, Optical spectrum of MoS₂: many-body effects and diversity of exciton states, *Phys. Rev. Lett.* **111**, 216805 (2013).
- [12] T. C. Berkelbach, M. S. Hybertsen, and D. R. Reichman, Theory of neutral and charged excitons in monolayer transition metal dichalcogenides, *Phys. Rev. B* **88**, 045318 (2013).
- [13] Andreas V. Stier, Kathleen M. McCreary, Berend T. Jonker, Junichiro Kono, and Scott A. Crooker, Exciton diamagnetic shifts and valley Zeeman effects in monolayer WS₂ and MoS₂ to 65 Tesla, *Nat. Commun.* **7**, 10643 (2016).
- [14] T. Yu and M. W. Wu, Valley depolarization due to intervalley and intravalley electron-hole exchange interactions in monolayer MoS₂, *Phys. Rev. B* **89**, 205303 (2014).
- [15] H. Yu, G. Liu, P. Gong, X. Xu and W. Yao, Dirac cones and Dirac saddle points of bright excitons in monolayer transition metal dichalcogenides, *Nat. Commun.* **5**, 3876 (2014).
- [16] Hanan Dery and Yang Song, Polarization analysis of excitons in monolayer and bilayer transition-metal dichalcogenides, *Phys. Rev. B* **92**, 125431 (2015).
- [17] Diana Y. Qiu, Ting Cao, and Steven G. Louie, Nonanalyticity, Valley quantum phases, and lightlike exciton dispersion in monolayer transition metal dichalcogenides: theory and first-principles calculations, *Phys. Rev. Lett.* **115**, 176801 (2015).
- [18] F. Wu, F. Qu, and A. H. MacDonald, Exciton band structure of monolayer MoS₂, *Phys. Rev. B* **91**, 075310 (2015).
- [19] T. Deilmann and K. S. Thygesen, Finite-momentum exciton landscape in mono- and bilayer transition metal dichalcogenides, *2D Mater.* **6**, 035003 (2019).
- [20] D. Y. Qiu, G. Cohen, D. Novichkova, and S. Refaely-Abramson, Signatures of Dimensionality and Symmetry in Exciton Band Structure: Consequences for Exciton Dynamics and Transport, *Nano Lett.* **21**, 7644 (2021).
- [21] A. Raja, L. Waldecker, J. Zipfel, Y. Cho, S. Brem, J. D. Ziegler, M. Kulig, T. Taniguchi, K. Watanabe, E. Malic et al., Dielectric disorder in two-dimensional materials, *Nat. Nanotechnol.* **14**, 832 (2019).
- [22] Y. Xu, S. Liu, D. A. Rhodes, K. Watanabe, T. Taniguchi, J. Hone, V. Elser, K. F. Mak, and J. Shan, Correlated insulating states at fractional fillings of moiré superlattices, *Nature (London)* **587**, 214 (2020).

- [23] Xu-Chen Yang, Hongyi Yu, and Wang Yao, Waveguiding valley excitons in monolayer transition metal dichalcogenides by dielectric interfaces in the substrate, *Phys. Rev. B* **104**, 245305 (2021).
- [24] Xu-Chen Yang, Hongyi Yu, and Wang Yao, Chiral Excitonics in Monolayer Semiconductors on Patterned Dielectrics, *Phys. Rev. Lett.* **128**, 217402 (2022).
- [25] Th. Forster, Energiewanderung und Fluoreszenz, *Naturwissenschaften* **33**, 166–175 (1946).
- [26] Hyun Dong Ha, Dong Ju Han, Jong Seob Choi, Minsu Park, Tae Seok Seo, Dual role of blue luminescent MoS_2 quantum dots in fluorescence resonance energy transfer phenomenon, *Small* **10**, 3858–62 (2014).
- [27] A. Hichri, T. Amand, and S. Jaziri, Resonance energy transfer from moiré-trapped excitons in $\text{MoSe}_2/\text{WSe}_2$ heterobilayers to graphene: Dielectric environment effect, *Phys. Rev. Materials* **5**, 114002 (2021).
- [28] Jie Zhou, Jiajie Chen, Yanqi Ge and Yonghong Shao, Two-dimensional nanomaterials for Förster resonance energy transfer-based sensing applications, *Nanophotonics* **9**, 7 (2020).
- [29] W. P. Su, J. R. Schrieffer, and A. J. Heeger, Solitons in Polyacetylene, *Phys. Rev. Lett.* **42**, 1698 (1979).
- [30] J. K. Asbóth, L. Oroszlány, and A. P. Pályi, *A Short Course on Topological Insulators* (Springer International Publishing, Switzerland, 2016).
- [31] M. Selig, E. Malic, K. J. Ahn, N. Koch, and A. Knorr, Theory of optically induced Förster coupling in van der Waals coupled heterostructures, *Phys. Rev. B* **99**, 035420 (2019).
- [32] L. C. Andreani and F. Bassani, Exchange interaction and polariton effects in quantum-well excitons. *Phys. Rev. B* **41**, 7536–7544 (1990).
- [33] See Supplementary for details regarding the electron-hole Coulomb exchange, and analysis of SSH chain.